Visible extreme adaptive optics on extremely large telescopes: Towards detecting oxygen in Proxima Centauri b and analogs

J. Fowler, Sebastiaan Y. Haffert, Maaike A.M. van Kooten, Rico Landman, Alexis Bidot, Adrien Hours, Mamadou N'Diaye, Olivier Absil, Lisa Altinier, Pierre Baudoz, Ruslan Belikov, Markus Johannes Bonse, Kimberly Bott, Bernhard Brandl, Alexis Carlotti, Sarah L. Casewell, Elodie Choquet, Nicolas B. Cowan, Niyati Desai, David Doelman, Kevin Fogarty, Timothy D. Gebhard, Yann Gutierrez, Olivier Guyon, Olivier Herscovici-Schiller, Roser Juanola-Parramon, Matthew Kenworthy, Elina Kleisioti, Lorenzo König, Mariya Krasteva, Iva Laginja, Lucie Leboulleux, Johan Mazoyer, Maxwell A. Millar-Blanchaer, David Mouillet, Emiel Por, Laurent Pueyo, Frans Snik, Dirk van Dam, Kyle van Gorkom, Sophia R. Vaughan

ABSTRACT

Looking to the future of exo-Earth imaging in visible light from the ground, core technology developments are required in visible extreme adaptive optics (exAO) to enable the observation of atmospheric features on rocky planets in this spectral range. UNDERGROUND (Ultra-fast AO techNology Determination for Exoplanet imageRs from the GROUND), a collaboration built in Feb. 2023 at the Optimal Exoplanet Imagers Lorentz Workshop, aims to: (1) set the instrumental requirements to detect Oxygen in Proxima Centauri b and analogs as an informative science case for high-contrast imaging and spectroscopy, (2) overview the state of the field with respect to visible exoplanet imagers, and (3) identify key technologies that require further development.

1. INTRODUCTION

Finding and characterizing exo-Earths is a key science goal of Extremely Large Telescope missions. To explore the diversity of substellar companions, understand the formation and evolution of planetary systems, and find clues about the presence of life outside our solar system. Unlike their gas giant-planet cousins, Earth analogs will have an extremely faint self-luminous glow in the near infrared (NIR); current and future ground-based visible to NIR exoplanet imagers will not be able to detect that thermal emission. To observe these rocky planets, we must detect the light them in reflected light from their host star.

Proxima Centauri is a promising stellar system for reflected light studies. Proxima Centauri A is an M dwarf at 1.29 pc from our solar system that hosts the Earth-like planet Proxima Centauri b.[1] Proxima Centauri b is a 1.3 $M_\oplus$ exoplanet,[1] famous for its proximity to Earth; our closeness to Proxima Centauri is favorable to study this system with coronagraphic observations, as planetary companions appear at large angular separations from their host star as we get closer to earth. For example, Proxima Centauri b has a maximum elongation of 38 milli-arcseconds (mas).[1] Such an orbit is in theory resolvable at visible wavelengths by current telescopes such as the VLT or Magellan ($\lambda_{O_2}/D = 19$ mas, and $\lambda_{O_2}/D = 24$ mas, respectively.) It will become even easier when we go to the next generation of extremely large telescopes. The resolution of the European Extremely Large Telescope (E-ELT) and the Giant Magellan Telescope are 4 mas and 6 mas, respectively.

While many spectral features indicate the disequlibrium chemistry that implies signs of life, oxygen has been thought to be one of the strongest biosignatures as it is the strongest marker of life in Earth's current atmosphere. The abundance of O_2 closely follows the presence of life that uses oxygenic photosynthesis mechanisms. While recent research has found that there are also several abiotic processes that can generate an O_2 signature, we still require the detection of O_2 as a prerequisite for the presence of life.[2] In this work we examine the requirements to detect oxygen in the atmosphere of Proxima Centauri b using ground-based telescopes.

In Section 2 we describe the current state of the field for visible light adaptive optics from the ground. In Section 3.1 we outline the required contrast to detect Oxygen in the atmosphere of Proxima Centauri b. In Section 3.2 we estimate a simplified AO wavefront error budget to determine the speed of the AO system before simulating the final contrast in Section 3.4. In Section 4 we suggest an instrument architecture and describe the remaining technology development required to reach it. Finally, in Section 5 we make our final conclusions.

2. STATE OF VISIBLE HIGH CONTRAST IMAGING FROM THE GROUND

There are currently only a handful of Extreme Adaptive Optics (ExAO) instruments that operate at visible wavelengths. These are VLT/SPHERE,[3] SUBARU/SCExAO[4] and Magellan/MagAO-X.[5,6] SPHERE/ZIMPOL, SCExAO/VAMPIRES and MagAO-X report raw contrasts on the order of $\sim 10^{-3}$ at 100 mas. The leading limitation in all systems are non common path aberrations (NCPA) which can be both static and quasi-static. Therefore, one of the most crucial developments is active focal plane wavefront control. Especially the algorithms that can control mid to high-spatial frequencies. Electric Field Conjugation (EFC) and implicit-EFC (iEFC) are examples of such dark hole digging algorithms 7, 8, 9. These have been proven to remove quasi-static aberrations to within $5 \cdot 10^{-8}$ in the lab 8 and $1 \cdot 10^{-6}$ on-sky 7. Atmospheric speckles are the ultimate limiting factor after the NPCA speckles have been removed.

Instrument	Contrast	Wavelength	Seeing	Ref
SPHERE/ZIMPOL	1e-3	I'	0.9"	[10]
SCExAO/VAMPIRES	5e-3	750 nm	0.55"*	[11]
MagAO-X	2e-3	I	0.75"	private communication

Table 1. State of the art for visible AO performance on large (8 meter class) telescopes. *The seeing for this measurement was not recorded so we have provided the median seeing for the Maunakea Summit.

3. CONTRAST REQUIREMENTS FOR DETECTING OXYGEN

3.1 Gain from high-dispersion spectroscopy

High-dispersion spectroscopy (HDS) can very efficiently filter out starlight. An exoplanet atmosphere is usually very different from that of its host star due to a difference in atomic and molecular abundances and pressure-temperature profiles. At a high enough spectral resolution we can disentangle planet and starlight by using matched filters.[12] The downside to using HDS is that we can only use the information content that is present in the spectral lines. The majority of the planet continuum is not different from that of its host star. Therefore, we lose all the continuum light. And even worse, at low spectral resolution it is not possible to disentangle starlight from planet light because stellar speckles have a similar spectral shape.[13] Therefore, we need to use a low-pass filter on the measured spectra to remove the influence of star light which will also remove almost all of the continuum flux of the planet. The efficiency of HDS is defined as the ratio between the signal after and before low-pass filtering.[13] The results for the oxygen A-band lines are shown in Figure 1. The calculation was done for a spectral bandwidth between 760 nm and 770 nm because that is the range for the oxygen A-band. The figure shows that the efficiency is highest at high spectral resolution, which has been shown in the past.[14–16] We assumed that we observe the system in the most optimistic time window where the influence of Earth's telluric lines are minimized.[14,15]

3.2 Contrast requirements

Our science case is the detection of the oxygen A-band in the atmosphere in Proxima b (centered at 765nm; 10nm bandwidth; 1e-7 contrast) within a single night of observation with the E-ELT. High-spectral resolution (R$= 2 \cdot 10^5$) observations are required to separate the Oxygen lines from Earth's telluric lines. The instrument will need simultaneous spectra of the star and planet for removing residual star light.

Because HRS (high resolution spectroscopy) is a photon-noise limited post-processing algorithm, SNR is calculated with:

$$\mathrm{SNR} = \frac{\eta T_p C F_s}{\sqrt{F_s K}} = \eta C T_p \sqrt{F_s / K}. \quad (1)$$

with efficiency of the post-processing η, throughput of the planet T_p, contrast between planet and star C, stellar flux F_s, and achieved raw contrast K. The main drivers for the SNR are η, T_p, and K.

For Proxima Centauri b we have the following parameters:

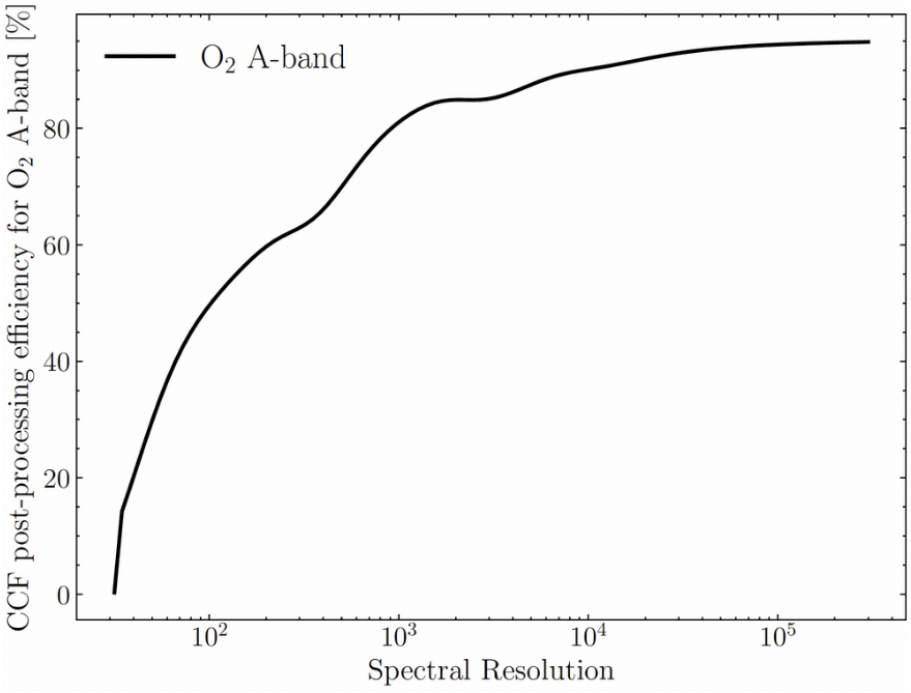

Figure 1. The efficiency of HRS post-processing (in this case we use a cross correlation function) as a function of spectral resolution. The efficiency converges to 95% around $R = 10^5$.

- Telescope area of ELT = 1058.32 m^2
- Contrast of Proxima Centauri b at $1 \cdot 10^{-7}$
- End-to-end throughput to spectrograph of 0.1
- The goal SNR is 5
- Efficiency of HDS η is 0.95 according to Figure 1.
- A spectral bandwidth of 10.0 nm (760 nm to 770 nm)
- The stellar magnitude of Proxima Centauri at I-band is 7.4
- A total integration time of 4 hours

With these parameters we arrive at a raw contrast requirement of $3 \cdot 10^{-5}$ at 10 λ/D to achieve SNR=5 in 4 hours of exposure time with HRS on the E-ELT.

3.3 Adaptive Optics Error Budget

We calculate a simplified AO wavefront error budget to investigate the effects of the time delay in the AO system (i.e., the servo-lag error) on the wavefront error and Strehl ratio. From our contrast estimated in Sec 3.2, we can estimate the required wavefront error (contrast is inversely proportional to the square of the wavefront error in radians for a given separation). Over the entire control radius we need to maintain a wavefront error around 45nm. Using TIPTOP[17] - an analytical AO modelling software- we determine the fitting error for a system using a deformable mirror (DM) with 200 actuators across the pupil. Here we make the choice of using roughly 200 actuators across the pupil to match the actuator pitch roughly to the Fried parameter expected for good seeing conditions on the E-ELT (r_0 = 20 cm). We then look at the effect of the servo-lag error on the total residual wavefront error and use that to estimate the Strehl ratio using the Marechal approximation. The largest error term is the fitting error which will be reduced for the best seeing conditions or with future technology that

further improves the actuator density on wavefront correctors such as a DM. Assuming the wavefront sensor aliasing is negligible by using an optimal wavefront sensor, the next largest error term is the servo-lag error. In Tab 2, we present the effects of these two terms while changing the speed of the AO system effectively tuning the servo-lag error. We are in a regime where reducing the servo-lag error provides an important improvement in SR allowing up to 90% SR when running at 5kHz assuming an effective wind velocity of 10m/s (again good atmospheric conditions). This shows that we need to run at approximately 2kHz to achieve a wavefront error smaller than 45nm rms and deliver high Strehl ratio to the coronagraph. While minimizing the wavefront error before the corongraph is important to achieving good contrast, we need to build on these simulations and look directly at the exact impact of the servo-lag error and our proposed system on the raw contrast; these results are shown in Sec 3.4.

Error term	1kHz	2kHz	5kHz
Fitting Error	38.92	38.92	38.92
Servo-lag Error	29.47	14.87	5.97
Total residual wavefront Error	48.8	41.7	39.38
SR (Marechal approx)	85%	89%	90%

Table 2. RMS (root mean square) wavefront error in nm for major error terms as we vary the control speed. Assuming a 39m telescope, natural guide star (not limited by SNR/guidestar magnitude), 0.5" seeing, effective wind velocity of 10 m/s, 200 actuators across the pupil, and loop delay of 1 frame, at 750 nm.

3.4 Contrast Curves at Varying AO Loop Speeds

A more detailed analysis of the performance was done by using a spatial-filter based semi-analytical approach[18,19] to model the AO performance. The semi-analytical approach models each aspect of the AO system as a spatial transfer function that acts onto the atmospheric PSDs. The final PSD is then propagated through coronagraph to get the achieved raw contrast. This is also done by using a semi-analytical approach which is a quick way to generate long-exposure PSFs.[20] The noise on each mode is,[21]

$$\sigma^2 = \frac{1}{s_{pn}^2 N} + \frac{N_{sub}\sigma_{rn}^2}{s_{rn}^2 N^2}. \tag{2}$$

With σ^2 the reconstructed wavefront variance, s_{pn} the sensitivity to photon noise, N_{sub} the number of pixels used for wavefront sensing, σ_{rn} the detector read noise, s_{rn} the read noise sensitivity and N the number of photons per frame. The pyramid wavefront sensor has a sensitivity of $1/\sqrt{2}$ for both photon noise and read noise.[19,22] We have neglected the effects of amplitude errors due to scintillation. We also assumed that there would be no chromatic errors because we are performing science and wavefront sensing at the same wavelength. The results of the model are shown in Figure 2. Here we see that we get the best contrast at small angular separations with a loop speed of 2 kHz. The aniso-server error dominates at the slower loop speed of 1 kHz and at high speeds the photon noise starts to dominate which degrades contrast. Therefore, the system should run at roughly 2 kHz for optimal performance. The controller is an optimal modal gain integral controller following.[19,23]

3.5 Improvements from predictive wavefront control methods

Above we have investigated the rate at which the AO system and NCPA correction would need to run to achieve our contrast goal. We have not, however, performed a photon budget analysis to determine if we will have enough signal-to-noise to run both of the loops at the desired rates. One strategy to allow the system to run slower while maintaining the high level of correction is to implement advanced control algorithms that optimize the control bandwidth. A potential solution is predictive control. On sky testing from Keck/NIRC2[24] shows predictive control can provide a factor of 2-3 in contrast as compared to an integrator when running at 1kHz. It is also possible to run the NCPA loop with a predictive step to further improve the correction.[25] With an arbitrarily bright guidestar, the performance improvements from predictive control theoretically lessen as the control speed increases but it can also help maintain the same performance while running the loop slower. However predictive control is likely also controlling for standard consistent vibrations and systematics, so may see some increased

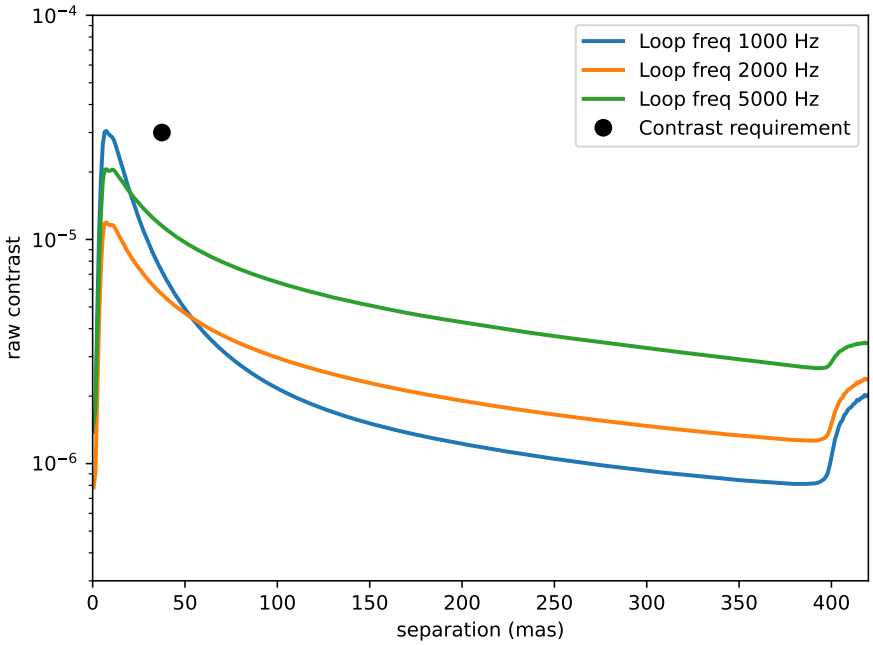

Figure 2. The contrast for various (1, 2, and 5 kHz) loop speeds for an unmodulated pyramid wavefront sensor (PWFS). The black dot illustrates the contrast requirement for the detection of Oxygen on Proxima Centauri b. Note that 2kHz AO provides the best correction at small angular separations.

performance regardless. Perhaps more importantly however, adaptive predictive control[26] will allow a system to constantly adapts it controller to provide optimal control.[?,27,28] This is important as the conditions during observations are constantly changing.[26]

3.6 NCPA Correction Speed

Independent of the AO system, wavefront errors exist in the system that degrade our final performance. Specifically NCPA's, whatever their origin, must be corrected for to achieve good contrast. To better understand how fast we would need to run an NCPA correct, we perform a case study using an existing instrument for which the NCPAs have been measured and characterised. We focus on VLT/SPHERE to determine how fast a NCPA wavefront sensor would need to run to correct for the NCPA detected by the ZELDA wavefront sensor.[29] From the NCPA decorelation equations found for SPHERE for a variety of different nights, we estimate the correction frequency of the NCPA correction loop for the best and worse case scenarios. If we want to keep the NCPAs below 1 nm rms wavefront error, to maintain a contrast of $3 \cdot 10^{-5}$, in the worse case we need to run the NCPA correction loop at 45 Hz as shown in Fig 3.

4. PROPOSED INSTRUMENT ARCHITECTURE

Here, we lay out our proposed instrument architecture for the UNDERGROUND instrument. We focus on 3 main technologies to mature: (1) optimal WFS at 1-2kHz, (2) fast NCPA control, and (3) high resolution spectroscopy. Figure 4 shows the proposed instrument design for the UNDERGROUND instrument.

Optimal WFS at 1-2kHz: We need a high-speed high-order sensitive wavefront sensor that will control the ExAO deformable mirror. This could be an un-modulated pyramid wavefront sensor[30] or the optimized ZWFS[21] or the optimal PIAA-ZWFS.[8] Depending on the wavefront sensor, we need a different amount of pixels to sample the wavefront. The pyramid WFS requires a detector that can run at least 440x440 pixels at 1-2 kHz with sub-electron read-noise. Recent advances in CMOS detector technology does show much promise. *.

*The Kinetix from Teledyne can run at 3.6 kHz in high-speed mode with 440 pixel lines

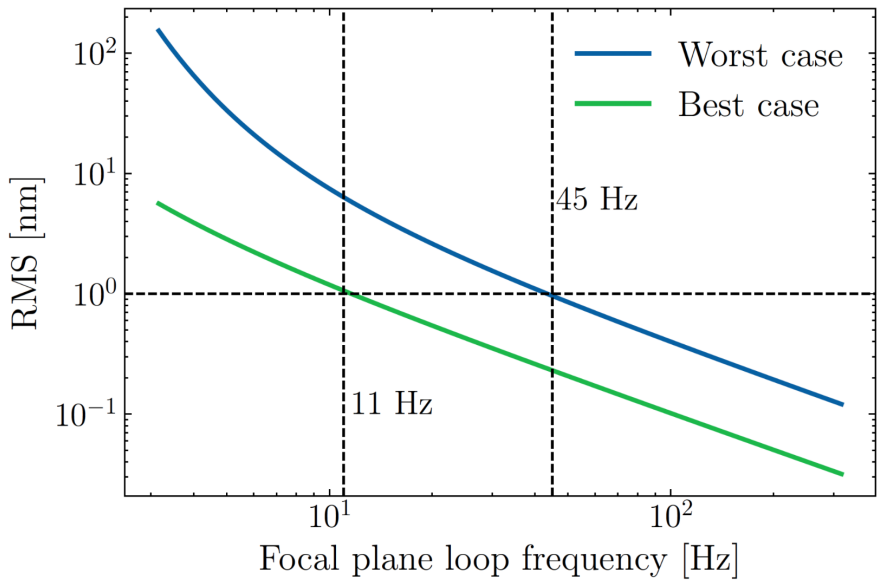

Figure 3. Examining required NCPA loop speed.

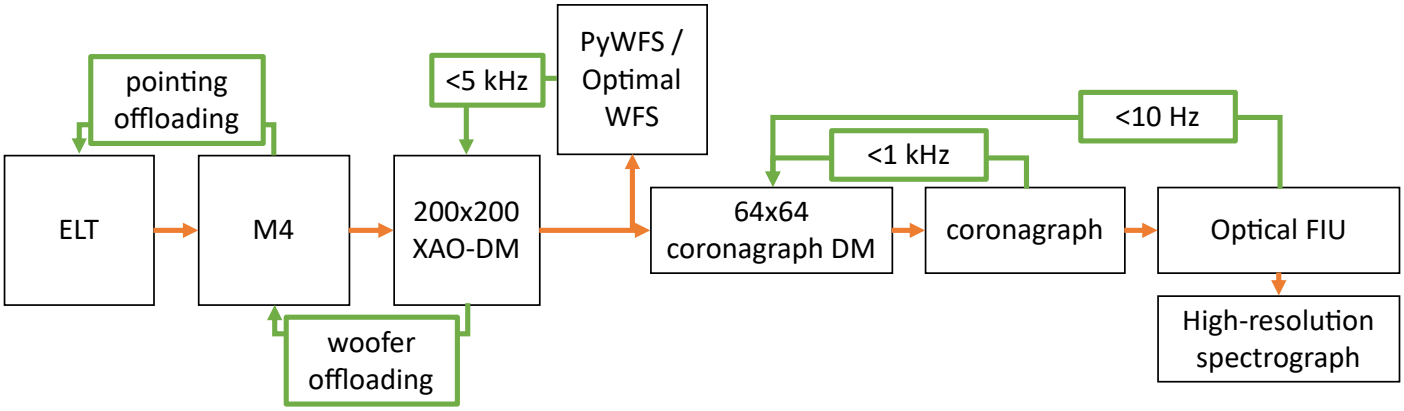

Figure 4. A schematic of the proposed UNDERGROUND instrument setup. A high-speed high-order loop is correcting the atmosphere to maintain high Strehl. A slow loop at 10 Hz will create a dark hole region where all starlight is nulled. This dark hole will be maintained at high speed by the wavefront sensor that is integrated into the coronagraph.

Fast NCPA Control: The NCPAs will be controlled by a WFS that is integrated into the coronagraph. This could be a ZWFS integrated within a Lyot-style coronagraph as demonstrated in.[?,?,8] The integrated control inside the coronagraph is necessary to meet the raw contrast requirements. Additionally, we added a dedicated corographic DM inside the instrument to control the focal plane speckles. This will make it easier to implement EFC or iEFC because there is no need anymore to reference offset the high-order wavefront sensor. This separates the control loops of both processes making it easier to control both.

High Resolution Spectroscopy: There are several attractive solutions for high-resolution multi-object spectrographs, especially if only a small narrow wavelength range is required. A promising one is the VIPA-style spectrograph[31,32] that can achieve high throughput and resolution in a compact design.

5. CONCLUSION

In conclusion, Proxima Centauri b provides an exciting opportunity to detect and characterize a earth-like planet in visible light. With high resolution spectroscopy, observations with ELTs could detect features like Oxygen

that point to life on other planets. With a contrast goal of 3×10^{-5} at 10λ/D, ground-based adaptive optics will likely achieve this, if we are able to do optimal wavefront sensing and control at $\geq$1kHz, fast NCPA control with integrated wavefront sensors and coronagraph, and efficient high-resolution multi-object spectroscopy.

ACKNOWLEDGMENTS

The workshop on which this manuscript is based was made possible thanks to the logistical and financial support of the Lorentz Center, Leiden, Netherlands. This workshop was supported by NOVA and the EXACT ERC (Grant agreement ID: 866001). YouName was funded by the RichPeople foundation for Finding Life in the Universe.

SYH was funded by the generous support of the Heising-Simons Foundation.

REFERENCES

[1] Anglada-Escudé, G., Amado, P. J., Barnes, J., Berdiñas, Z. M., Butler, R. P., Coleman, G. A. L., de La Cueva, I., Dreizler, S., Endl, M., Giesers, B., Jeffers, S. V., Jenkins, J. S., Jones, H. R. A., Kiraga, M., Kürster, M., López-González, M. J., Marvin, C. J., Morales, N., Morin, J., Nelson, R. P., Ortiz, J. L., Ofir, A., Paardekooper, S.-J., Reiners, A., Rodríguez, E., Rodríguez-López, C., Sarmiento, L. F., Strachan, J. P., Tsapras, Y., Tuomi, M., and Zechmeister, M., "A terrestrial planet candidate in a temperate orbit around Proxima Centauri," *Nature* **536**, 437–440 (Aug. 2016).

[2] Meadows, V. S., Reinhard, C. T., Arney, G. N., Parenteau, M. N., Schwieterman, E. W., Domagal-Goldman, S. D., Lincowski, A. P., Stapelfeldt, K. R., Rauer, H., DasSarma, S., et al., "Exoplanet biosignatures: understanding oxygen as a biosignature in the context of its environment," *Astrobiology* **18**(6), 630–662 (2018).

[3] Beuzit, J. L., Vigan, A., Mouillet, D., Dohlen, K., Gratton, R., Boccaletti, A., Sauvage, J. F., Schmid, H. M., Langlois, M., Petit, C., Baruffolo, A., Feldt, M., Milli, J., Wahhaj, Z., Abe, L., Anselmi, U., Antichi, J., Barette, R., Baudrand, J., Baudoz, P., Bazzon, A., Bernardi, P., Blanchard, P., Brast, R., Bruno, P., Buey, T., Carbillet, M., Carle, M., Cascone, E., Chapron, F., Charton, J., Chauvin, G., Claudi, R., Costille, A., De Caprio, V., de Boer, J., Delboulbé, A., Desidera, S., Dominik, C., Downing, M., Dupuis, O., Fabron, C., Fantinel, D., Farisato, G., Feautrier, P., Fedrigo, E., Fusco, T., Gigan, P., Ginski, C., Girard, J., Giro, E., Gisler, D., Gluck, L., Gry, C., Henning, T., Hubin, N., Hugot, E., Incorvaia, S., Jaquet, M., Kasper, M., Lagadec, E., Lagrange, A. M., Le Coroller, H., Le Mignant, D., Le Ruyet, B., Lessio, G., Lizon, J. L., Llored, M., Lundin, L., Madec, F., Magnard, Y., Marteaud, M., Martinez, P., Maurel, D., Ménard, F., Mesa, D., Möller-Nilsson, O., Moulin, T., Moutou, C., Origné, A., Parisot, J., Pavlov, A., Perret, D., Pragt, J., Puget, P., Rabou, P., Ramos, J., Reess, J. M., Rigal, F., Rochat, S., Roelfsema, R., Rousset, G., Roux, A., Saisse, M., Salasnich, B., Santambrogio, E., Scuderi, S., Segransan, D., Sevin, A., Siebenmorgen, R., Soenke, C., Stadler, E., Suarez, M., Tiphène, D., Turatto, M., Udry, S., Vakili, F., Waters, L. B. F. M., Weber, L., Wildi, F., Zins, G., and Zurlo, A., "SPHERE: the exoplanet imager for the Very Large Telescope," *Astron. & Astrophys.* **631**, A155 (Nov. 2019).

[4] Jovanovic, N., Martinache, F., Guyon, O., Clergeon, C., Singh, G., Kudo, T., Garrel, V., Newman, K., Doughty, D., Lozi, J., et al., "The subaru coronagraphic extreme adaptive optics system: enabling high-contrast imaging on solar-system scales," *Publications of the Astronomical Society of the Pacific* **127**(955), 890 (2015).

[5] Males, J. R., Close, L. M., Miller, K., Schatz, L., Doelman, D., Lumbres, J., Snik, F., Rodack, A., Knight, J., Van Gorkom, K., et al., "Magao-x: project status and first laboratory results," in [*Adaptive Optics Systems VI*], **10703**, 76–89, SPIE (2018).

[6] Close, L. M., Males, J. R., Durney, O., Sauve, C., Kautz, M., Hedglen, A., Schatz, L., Lumbres, J., Miller, K., Van Gorkom, K., et al., "Optical and mechanical design of the extreme ao coronagraphic instrument magao-x," in [*Adaptive Optics Systems VI*], **10703**, 1227–1236, SPIE (2018).

[7] Potier, A., Mazoyer, J., Wahhaj, Z., Baudoz, P., Chauvin, G., Galicher, R., and Ruane, G., "Increasing the raw contrast of VLT/SPHERE with the dark hole technique. II. On-sky wavefront correction and coherent differential imaging," *Astron. & Astrophys.* **665**, A136 (Sept. 2022).

[8] Haffert, S. Y., Males, J. R., Ahn, K., Van Gorkom, K., Guyon, O., Close, L. M., Long, J. D., Hedglen, A. D., Schatz, L., Kautz, M., Lumbres, J., Rodack, A., Knight, J. M., and Miller, K., "Implicit electric field conjugation: Data-driven focal plane control," *Astron. & Astrophys.* **673**, A28 (May 2023).

[9] Ahn, K., Guyon, O., Lozi, J., Vievard, S., Deo, V., Skaf, N., Bragg, J. C., Haffert, S. Y., Males, J. R., and Currie, T., "Combining EFC with spatial LDFC for high-contrast imaging on Subaru/SCExAO," *Astron. & Astrophys.* **673**, A29 (May 2023).

[10] Schmid, H. M., Bazzon, A., Roelfsema, R., Mouillet, D., Milli, J., Menard, F., Gisler, D., Hunziker, S., Pragt, J., Dominik, C., et al., "Sphere/zimpol high resolution polarimetric imager-i. system overview, psf parameters, coronagraphy, and polarimetry," *Astronomy & Astrophysics* **619**, A9 (2018).

[11] Lucas, M., Bottom, M., Guyon, O., Lozi, J., Norris, B., Deo, V., Vievard, S., Ahn, K., Skaf, N., and Tuthill, P., "A visible-light Lyot coronagraph for SCExAO/VAMPIRES," in [*Ground-based and Airborne Instrumentation for Astronomy IX*], Evans, C. J., Bryant, J. J., and Motohara, K., eds., *Society of Photo-Optical Instrumentation Engineers (SPIE) Conference Series* **12184**, 121844E (Aug. 2022).

[12] Snellen, I., de Kok, R., Birkby, J., Brandl, B., Brogi, M., Keller, C., Kenworthy, M., Schwarz, H., and Stuik, R., "Combining high-dispersion spectroscopy with high contrast imaging: Probing rocky planets around our nearest neighbors," *Astronomy & Astrophysics* **576**, A59 (2015).

[13] Landman, R., Snellen, I., Keller, C., N'Diaye, M., Fagginger-Auer, F., and Desgrange, C., "Trade-offs in high-contrast integral field spectroscopy for exoplanet detection and characterisation: Young gas giants in emission," *arXiv preprint arXiv:2305.19355* (2023).

[14] Rodler, F. and López-Morales, M., "Feasibility studies for the detection of o2 in an earth-like exoplanet," *The Astrophysical Journal* **781**(1), 54 (2014).

[15] Serindag, D. B. and Snellen, I. A., "Testing the detectability of extraterrestrial o2 with the extremely large telescopes using real data with real noise," *The Astrophysical Journal Letters* **871**(1), L7 (2019).

[16] Hardegree-Ullman, K. K., Apai, D., Bergsten, G. J., Pascucci, I., and López-Morales, M., "Bioverse: A comprehensive assessment of the capabilities of extremely large telescopes to probe earth-like o2 levels in nearby transiting habitable-zone exoplanets," *The Astronomical Journal* **165**(6), 267 (2023).

[17] Neichel, B., Beltramo-Martin, O., Plantet, C., Rossi, F., Agapito, G., Fusco, T., Carolo, E., Carla, G., Cirasuolo, M., and van der Burg, R., "Tiptop: a new tool to efficiently predict your favorite ao psf," (2021).

[18] Jolissaint, L., "Synthetic modeling of astronomical closed loop adaptive optics," *arXiv preprint arXiv:1009.1581* (2010).

[19] Males, J. R. and Guyon, O., "Ground-based adaptive optics coronagraphic performance under closed-loop predictive control," *Journal of Astronomical Telescopes, Instruments, and Systems* **4**(1), 019001–019001 (2018).

[20] Herscovici-Schiller, O., Mugnier, L. M., and Sauvage, J.-F., "An analytic expression for coronagraphic imaging through turbulence. application to on-sky coronagraphic phase diversity," *Monthly Notices of the Royal Astronomical Society: Letters* **467**(1), L105–L109 (2017).

[21] Chambouleyron, V., Fauvarque, O., Sauvage, J. F., Dohlen, K., Levraud, N., Vigan, A., N'Diaye, M., Neichel, B., and Fusco, T., "Variation on a Zernike wavefront sensor theme: Optimal use of photons," *Astron. & Astrophys.* **650**, L8 (June 2021).

[22] Guyon, O., "Limits of adaptive optics for high-contrast imaging," *The Astrophysical Journal* **629**(1), 592 (2005).

[23] Gendron, E. and Léna, P., "Astronomical adaptive optics. ii. experimental results of an optimized modal control.," *Astronomy and Astrophysics Supplement, v. 111, p. 153* **111**, 153 (1995).

[24] van Kooten, M. A., Jensen-Clem, R., Cetre, S., Ragland, S., Bond, C. Z., Fowler, J., and Wizinowich, P., "Predictive wavefront control on keck ii adaptive optics bench: on-sky coronagraphic results," *Journal of Astronomical Telescopes, Instruments, and Systems* **8**(2), 029006–029006 (2022).

[25] Gerard, B. L., Perez-Soto, J., Chambouleyron, V., van Kooten, M. A. M., Dillon, D., Cetre, S., Jensen-Clem, R., Fu, Q., Amata, H., and Heidrich, W., "Various wavefront sensing and control developments on the Santa Cruz Extreme AO Laboratory (SEAL) testbed," in [*Adaptive Optics Systems VIII*], Schreiber, L., Schmidt, D., and Vernet, E., eds., **12185**, 121852H, International Society for Optics and Photonics, SPIE (2022).

[26] van Kooten, M., Doelman, N., and Kenworthy, M., "Impact of time-variant turbulence behavior on prediction for adaptive optics systems," *J. Opt. Soc. Am. A* **36**, 731–740 (May 2019).

[27] Haffert, S. Y., Males, J. R., Close, L. M., Van Gorkom, K., Long, J. D., Hedglen, A. D., Guyon, O., Schatz, L., Kautz, M., Lumbres, J., et al., "Data-driven subspace predictive control of adaptive optics for high-contrast imaging," *Journal of Astronomical Telescopes, Instruments, and Systems* **7**(2), 029001–029001 (2021).

[28] Landman, R., Haffert, S. Y., Radhakrishnan, V. M., and Keller, C. U., "Self-optimizing adaptive optics control with reinforcement learning for high-contrast imaging," *Journal of Astronomical Telescopes, Instruments, and Systems* **7**(3), 039002–039002 (2021).

[29] Vigan, A., Dohlen, K., N´Diaye, M., Cantalloube, F., Girard, J. H., Milli, J., Sauvage, J.-F., Wahhaj, Z., Zins, G., Beuzit, J.-L., Caillat, A., Costille, A., Le Merrer, J., Mouillet, D., and Tourenq, S., "Calibration of quasi-static aberrations in exoplanet direct-imaging instruments with a zernike phase-mask sensor - iv. temporal stability of non-common path aberrations in vlt/sphere," *A&A* **660**, A140 (2022).

[30] Ragazzoni, R., Diolaiti, E., and Vernet, E., "A pyramid wavefront sensor with no dynamic modulation," *Optics communications* **208**(1-3), 51–60 (2002).

[31] Zhu, X., Lin, D., Hao, Z., Wang, L., and He, J., "A VIPA Spectrograph with Ultra-high Resolution and Wavelength Calibration for Astronomical Applications," *Astronomical Journal* **160**, 135 (Sept. 2020).

[32] Carlotti, A., Bidot, A., Mouillet, D., Correia, J.-J., Jocou, L., Curaba, S., Delboulbé, A., Le Coarer, E., Rabou, P., Bourdarot, G., et al., "On-sky demonstration at palomar observatory of the near-ir, high-resolution vipa spectrometer," in [*Ground-based and Airborne Instrumentation for Astronomy IX*], **12184**, 523–543, SPIE (2022).